Biosensors and Bioelectronics 128 (2019) 129–136

Contents lists available at ScienceDirect

Biosensors and Bioelectronics

journal homepage: www.elsevier.com/locate/bios

Electrochemiluminescence sensor based on upconversion nanoparticles and oligoaniline-crosslinked gold nanoparticles imprinting recognition sites for the determination of dopamine

Ying Gu[a], Junping Wang[a,*], Haipeng Shi[a], Mingfei Pan[a], Bing Liu[a], Guozhen Fang[a], Shuo Wang[b,*]

[a] State Key Laboratory for Food Nutrition and Safety; College of Food Engineering and Biotechnology, Tianjin University of Science and Technology, Tianjin 300457, China
[b] Medical College, Nankai University, 300350 Tianjin, China

ARTICLE INFO

Keywords:
Electrochemiluminescence
Covalent organic frameworks
Oligoaniline-crosslinked gold nanoparticles
Electroconductibility molecular imprinting polymer
Dopamine

ABSTRACT

For the determination of dopamine (DA) in serum samples, a quenching-type electrochemiluminescence sensor (MIECLS) was constructed in this study. Upconversion nanoparticles (UCNPs) enhanced by covalent organic frameworks (COFs)-based hybrid and oligoaniline-crosslinked gold nanoparticles (AuNPs) imprinting recognition sites were introduced in electrochemiluminescence (ECL) system at the first time. The porous COFs-based hybrid with large specific surface area was modified on the electrode firstly to hold more UCNPs and imprinting recognition sites. AuNPs was employed in the developed sensor for two objectives: 1) AuNPs on the COFs-based hybrid enabled the hybrid to tunnel the electrons, which helped to improve the ECL intensity; 2) AuNPs-based thioaniline units (PATP@AuNPs) electropolymerized on the electrode in the presence of template to form oligoaniline-crosslinked AuNPs matrix. Then the exclusion of template from matrix yielded the molecularly three-dimensional imprinted contours with conductivity, which facilitated specific recognition and further amplified the ECL. The double recognition mode in this work involves the recognition effect of imprinted contours and quenching effect of *o*-benzoquinone species. The quantum chemical calculation was performed to analyze the possible recognition and the binding mechanisms of molecularly three-dimensional imprinted contours. The results showed imprinted contours could bind the targets by complementary spatial cavities and weak interactions. The proposed approach yielded a wide detection range (10^{-14}–10^{-6} M), low limit of detection (LOD = 2×10^{-15} M) and acceptable recoveries (93.25–112.97%) in rat serum sample, demonstrating that the developed method holds great promise to be applied to DA detection in practical samples.

1. Introduction

Electrochemiluminescence (ECL) is electro-generation luminescence technology controlled by the applied potential on electrodes (Wang et al., 2017), which is attractive in clinical diagnosis, environmental monitoring, pharmaceutical and food analysis, given its low-cost, low background emission, and high sensitivity (Yang et al., 2017). Generally, the generation principle of ECL involves the emission of the light arising from the high-energy electron-transfer reaction of the electro-generated reagents at the surface of the electrodes (Yang et al., 2016). ECL emitters play an essential part in ECL system. Heretofore, various luminophores have been served as ECL emitters and applied in ECL systems, including luminol, metal nanoclusters, Ru composites, and semiconductor quantum dots (L. Zhao et al., 2016a). Upconversion nanoparticles (UCNPs) is a kind of lanthanide-doped nanomaterials with anti-Stokes optical properties which can convert near-infrared (NIR) light into visible radiation via a nonlinear optical process (Jo et al., 2016). Taking advantage of the merits such as low toxicity, fine biocompatibility, deep NIR light penetration into tissue, and less photobleaching (Wu et al., 2015), UCNPs as a promising luminescent material has been increasingly applied in bioanalysis and in-vivo imaging. The high intensity, favorable chemical and optical stability, and stable cathodic signals of UCNPs (Guo et al., 2016), as compared to the common downconversion nanomaterials, help it to serve as ECL emitter and develop UCNPs-based ECL platform (Huang et al., 2012). Particularly, the joint use of UCNPs and advanced materials with favorable electrochemical performance could further improve its ECL property.

Covalent organic frameworks (COFs), a new type of crystalline porous material constructed from lightweight elements (B, N, C, and O etc.), are well known for the application in gas storage, catalysis and photoelectricity fields (Pachfule et al., 2014). COFs materials hold numerous merits such as permanent porosity, large specific surface areas,

* Corresponding authors.
E-mail addresses: wangjp@tust.edu.cn (J. Wang), wangshuo@nankai.edu.cn (S. Wang).

https://doi.org/10.1016/j.bios.2018.12.043

Available online 27 December 2018

low density and high stability, due to its highly ordered structures linked by strong covalent bonds (Ding et al., 2011). The ordered and porous structure of the COFs enables it to serve as a support with great load capacity (Liu et al., 2016). Gold nanoparticles (AuNPs) demonstrate significant merits emerging from the nanoscale dimensions and favorable electronic transmission capacity of the building blocks on the electrochemical sensing interface. COFs were modified with AuNPs to obtain the hybrid conducive to UCNPs emitter ECL system in present study.

The exploration of recognition elements to increase the binding capacity towards target is another concern to boost sensing performance of sensor (Zhong et al., 2015). In the recent years, molecularly imprinted polymers (MIP) with recognition sites complementary in shape and cavities with the templates offer a promising approach to construct new generation of recognition elements for sensing field (Jiang et al., 2015). Molecularly imprinted electrochemiluminescence sensor (MIECLS) combined MIP with ECL, demonstrating rapidity, specificity, high sensitivity, favorable stability, less-analyte required and ease of miniaturization, provides the ideal platform for sensing analysis (Jin et al., 2018). Additionally, the preparation of MIP by one-pot electro-polymerization on the electrodes could simplify the synthesis process and improve the controllability of polymer film (Sheikhzadeh et al., 2016). The poor conductibility and fewer valid imprinted recognition sites of conventional MIP, however, weaken its electrochemical signal and degrade the sensing performance to a great extent (Zhang et al., 2017). Improvement of MIP, especially reasonable innovation of functional monomer, could ameliorate the above demerits efficiently. Herein, the restructuring of MIP involves the generation of AuNPs-based imprinting recognition sites. AuNPs-based thioaniline units (PATP@AuNPs) could electropolymerize on the electrodes (Zhang et al., 2017) in the presence of the templates and form oligoaniline-crosslinked AuNPs matrix (PATP@AuNPs-crosslinked MIP). The aggregation of AuNPs is able to provide three-dimensional conductivity for electrochemical sensing (Riskin et al., 2008). Aniline unit can bridge AuNPs to assist the generation of three-dimensional oligoaniline-crosslinked AuNPs imprinting recognition sites to realize specific binding of target (Yildiz et al., 2008). Additionally, the larger specific surface area provided by COFs material modified electrode generates more valid imprinted recognition sites of MIP and improves sensing efficiency to a certain level.

Dopamine (DA) is a neurotransmitter which exerts crucial function on mammalian central nervous systems and endocrine system (Li et al., 2016). The sensitive detection and quantification of DA is of significance for the diagnoses, prevention and treatments of DA-related neurological disorders such as Alzheimer's disease, Huntington's disease, Tourette's syndrome, Parkinson's disease, and Schizophrenia (Anirudhan et al., 2014). Up to now, different analytical methods of DA have been reported including high performance liquid chromatography, visible spectrophotometry, colorimetric detection and the like (Anirudhan et al., 2014). In view of the defects suffering from conventional detection process such as high cost, long analysis time and complex pretreatment, further development of performance-improved detection methods for DA detection is highly desired.

Here, a quenching-type MIECLS was constructed for the determination of DA. UCNPs was employed as ECL emitter in this sensing system. The novel COFs-based ECL enhancement material (CTpBD-Au) and oligoaniline-crosslinked AuNPs imprinting recognition sites were introduced in ECL system at the first time. AuNPs loaded on COFs material acted as the carrier of electronic transfer to enhance ECL response. The CTpBD-Au with extra specific surface area held more UCNPs and crosslinked PATP@AuNPs, assisting the ECL response of UCNPs and providing more imprinted recognition sites. Furthermore, the ECL sensing effect was further enhanced by the assistance of three-dimensional molecularly imprinted contours and the conductivity of PATP@AuNPs-crosslinked MIP matrix. The functional monomers (PATP@AuNPs) on electrodeposited PATP@AuNPs-crosslinked MIP contours bound with DA through multiple weak interactions which were theoretically speculated by quantum chemical calculation. The formed molecularly imprinted contours specifically recognized the target by complementary spatial cavities and weak interactions, thus further causing the ECL quenching by energy-transfer process. The combination of the recognition effect and the quenching effect endowed a double recognition effect to DA sensing. The proposed approach displayed sensitive responses to DA and was successfully applied to the analysis of serum samples.

2. Experimental

2.1. Chemicals and apparatus

1, 3, 5-triformylphloroglucinol (Tp), diglycolic anhydride, and benzidine (BD) were purchased from Aladdin (Shanghai, China). 1,4-dioxane, dopamine, ascorbic acid (AA) and uric acid (UA) were obtained from Alfa Aesar (Tianjin, China). Gold chloride ($HAuCl_4$), caffeic acid, adrenaline and α-phenylethylamine (PEA) were purchased from Sigma-Aldrich (St. Louis, MO, USA). *p*-aminothiophenol (PATP) was supplied by Macklin Biochemical Co.,Ltd (Shanghai, China). And 2-mercaptoethane sulfonic acid was obtained from J&K Scientific Ltd. (Beijing, China). Tetrahydrofuran (THF) and ethanol absolute were purchased from Sinopharm Chemical Reagent Co.,Ltd (Tianjin, China). SiO_2-NH_2 modified upconversion nanoparticles ($NaYF_4$:Yb,Tm) was supplied by Fluonano Biotech Co.,Ltd (Hefei, China).

All electrochemical analysis was carried out by LK5100 ECL analyzer (Tianjin Lanlike Chemical and Electronic High Technology Co., Ltd., China). Fluorescence spectra were tested by an F-2500 fluorescence spectrophotometer (Hitachi, Japan) with an external 980 nm exciter. Fourier transfer infrared spectrum was obtained on Tensor 27 (Bruke, Germany). Morphology of materials and modified electrodes were characterized by transmission electron microscopy (TEM, JEM-2010FEF, JEOL, Japan) and scanning electron microscopy (SEM, JSM-IT300, JEOL, Japan), respectively.

2.2. Quantum chemical calculation

The model of the template–monomer complexes was set up. The structures of template and monomers were optimized theoretically by dint of density functional theory (DFT) via ORCA 4.0.1 (Neese, 2012). All wavefunction analyses were finished by Multiwfn 3.5 (Lu and Chen, 2012) and the color mapped isosurface images of electrostatic potential (ESP) and the Gradient Model (IGM) were rendered by VMD 1.9.3 program (Humphrey et al., 1996). IGM, a very intuitive way of examining weak intermolecular interactions, provides an uncoupling scheme that automatically separates intra- from inter-fragment interactions (Lefebvre et al., 2017). Here, the functional monomers were defined as the host and target was defined as the guest molecule. The weak interactions between them were studied by IGM. ESP-mapped molecular van der Waals (vdW) surface images were used to assess electrostatic potential of molecules. Basis set superposition errors (BSSE) was corrected by the geometrical counterpoise correction (gCP).

2.3. Fabrication of PATP@AuNPs-crosslinked MIP-based ECL sensors

Specific preparation methods of the CTpBD-Au and PATP@AuNPs were shown in Supplementary material. The fabrication of PATP@AuNPs-crosslinked MIP-based ECL sensors was depicted in Scheme 1. The bare GCE was polished and rinsed by deionized water before use. 10 mg CTpBD-Au was dispersed in ethanol solution and then mixed with 0.1% chitosan solution at same volume evenly. 10 μL mixture was dropped on the GCE and dried naturally for further research. Then, the 10 μL UCNPs solution (0.5 mg mL^{-1}) was dropped on CTpBD-Au/GCE surface and dried at room temperature. Electro-polymerization solution containing 0.1 mg mL^{-1} DA and 0.3 mg mL^{-1} of PATP-AuNPs in PBS

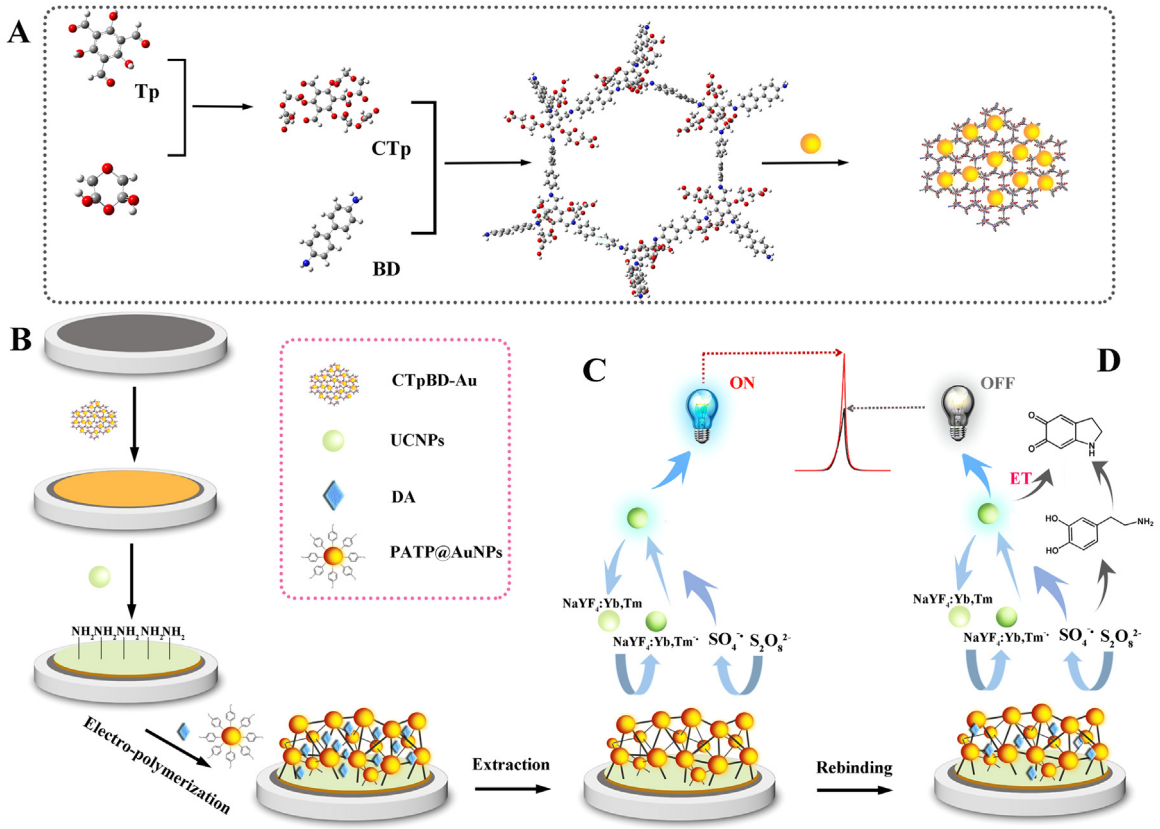

Scheme 1. Schematic illustration of (A) the fabrication process of CTpBD-Au hybrid and (B) the preparation and detection process of developed MIECLS ; (C) the light-emitting mechanism of ECL system; (D) the quenching mechanism of ECL.

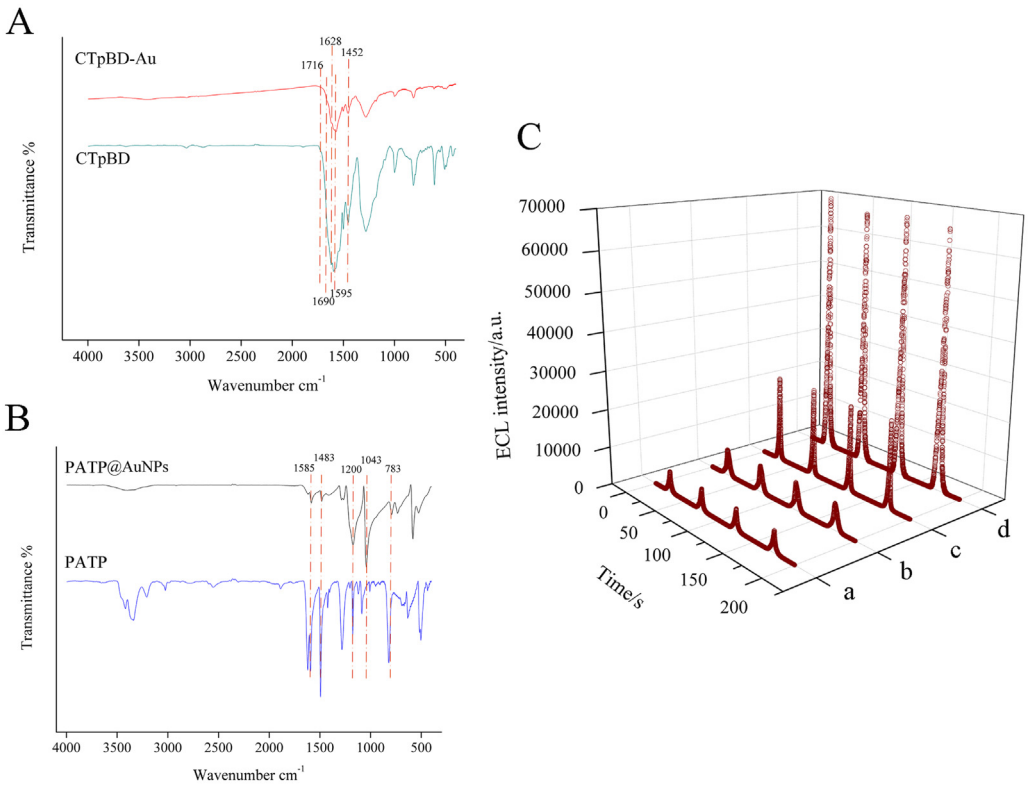

Fig. 1. FT-IR spectra of (A) CTpBD-Au and CTpBD, (B) PATP@AuNPs and PATP; (C) ECL curves of different modified electrodes: bare GCE (a), CTpBD-Au/GCE (b), UCNPs/GCE (c) and UCNPs/CTpBD-Au/GCE (d).

(0.01 M, pH = 7.4) was firstly pre-assembly for 3 h under nitrogen. Then PATP@AuNPs-crosslinked MIP film was prepared on UCNPs/CTpBD-Au/ GCE by the electro-polymerization at a constant potential of 1.0 V for 400 s (Xue et al., 2013). The extraction of the bound DA on modified electrode was conducted by washing in 0.01 M PBS (pH = 7.4) with continuous stirring for 15 min. For the control experiment, the non-imprinted electrochemiluminescence sensor (NIECLS) was fabricated with the same electro-polymerization condition as MIP-based electrode but without the addition of DA.

2.4. ECL measurement

The prepared MIP/UCNPs/CTpBD-Au/GCE was dipped in the DA solution of different concentrations for 8 min to rebind the target. The ECL measurement was performed in 0.1 M $K_2S_2O_8$ (0.1 M PBS, pH = 7.4) containing 0.1 M KCl and with a scanned potential from 0 V to −2.2 V at the scan rate of 100 mV s^{-1}. The voltage of the photomultiplier tube (PMT) applied was placed at 800 V. And the cyclic voltammetry (CV) and ECL were recorded simultaneously.

3. Results and discussion

3.1. Material characterization

The employed materials were characterized by TEM and FT-IR. The finely distributed 30 ± 2 nm sized UCNPs was clearly visible (Fig. S1A) in the TEM analysis and the circular core-shell structure illustrated that the SiO_2-NH_2 functional layer was well modified on the bare UCNPs. Fig. S1B is the TEM of CTpBD COFs which showed the typical lamellar structure as reported (Liu et al., 2018) and it can be observed the striking contrast between CTpBD and CTpBD-Au (Fig. S1C) that the loaded AuNPs (with average size about 5 nm) dispersed in CTpBD uniformly. Inset in Fig. S1C shows the enlarged view of CTpBD-Au. In FT-IR spectra (Fig. 1A), the peaks at the wavenumbers of ~1595, ~1452 and ~1628 cm^{-1} corresponded to the C=C, Ar (C=C), and C-N of the CTpBD, respectively. The appearances of C=O at ~1716 cm^{-1} of the ester on CTp as well as C=O at ~1690 cm^{-1} of carboxyl implied the successful construction of the CTpBD structure (Qian et al., 2016). The characteristic peaks of CTpBD shown in the FT-IR spectrum of CTpBD-AuNPs confirmed that the strong reaction with $NaBH_4$ could not destroy the chemical bond of the CTpBD framework. Fig. S1D reflects the high dispersity and homogeneity of as-synthesized PATP@AuNPs and the average particle size of the particles was 3.5 ± 0.5 nm which coincides with the previous report (Yang et al., 2016). Inset in Fig. S1D shows the enlarged view of PATP@AuNPs. The FT-IR spectrum of PATP was compared to that of PATP@AuNPs in Fig. 1B. The absorption peaks centered at ~1483 cm^{-1} and ~1585 cm^{-1} corresponding to the benzene ring frame vibration and peak located at ~783 cm^{-1} deriving from the benzene fingerprint region (Jiang et al., 2015). The bands at ~1043 cm^{-1} and ~1200 cm^{-1} were attributed to the absorption of sulfonate. The main peaks of PATP presenting in both FT-IR spectra testified that the PATP were validly coated on AuNPs.

3.2. Morphological characterization and ECL behaviors of different modified electrodes

The surface morphologies of different as-prepared modified electrodes were evaluated by SEM (Fig. S2). CTpBD-Au/GCE (Fig. S2A) possessed wrinkled and porous structure. After the modification of UCNPs (Fig. S2B), the electrode surface was covered with round particles uniformly. And the electro-polymerization of PATP@AuNPs-crosslinked MIP caused the further changes of the electrode surface. Fig. S2C clearly shows the rough and compact MIP matrix coated on UCNPs/CTpBD-Au/GCE. ECL curves (Fig. 1C) of bare GCE (a), CTpBD-Au/GCE (b), UCNPs/GCE (c) and UCNPs/CTpBD-Au/GCE (d) were obtained in 0.1 M $K_2S_2O_8$ solution (0.1 M PBS, pH = 7.4). The bare GCE only aroused a weak ECL intensity (~5453 a.u.). Compared with the bare GCE, the ECL intensity of CTpBD-Au/GCE reached ~6814 a.u. due to better electron-transfer of the hybrid. UCNPs here served as ECL emitter, and the ECL intensity of UCNPs/GCE (~23526 a.u.) was 4.3-fold or so as high as that of the bare GCE. UCNPs/CTpBD-Au/GCE showed the highest ECL intensity (~65886 a.u.) which was 12-fold or so than the bare GCE after the introduction of CTpBD-Au and UCNPs. As for the reason of the ECL enhancement, for one thing, the loading of AuNPs on the porous CTpBD could facilitate electron transport between electrode surface and UCNPs. And CTpBD-Au with higher specific surface area, for another, carries more UCNPs which gives full play to the superiority on assisting ECL.

3.3. PATP@AuNPs-crosslinked MIP-based ECL sensors and optimization

The PATP@AuNPs unit acted as functional monomers electropolymerized on the electrode in the presence of DA and subsequently templates were removed from the as-prepared PATP@AuNPs-crosslinked matrix, resulting in the formation of molecularly imprinted contours that could bind the target by complementary spatial cavities and weak interactions. The weak interactions between templates and monomers cover multiple different interactions. Fig. 2A-C show the IGM images of molecules at different views to simulate the possible interaction between templates and monomers. The green regions indicated possible weak vdW-type interactions (volume cutoff of δginter = 0.006). It can be seen from Fig. 2, a and i regions corresponded to S-H which could be explained by ESP-mapped molecular vdW surface images in Fig. 2D. The sites possessing opposite ESP possibly attract each other. The mutual penetration of red and blue regions (k) suggested the electrostatic attraction between S and H atoms. b region was π-π stacking dominated by dispersion force. And c, g and d, h were hydrogen bonds between N, H atoms and O, H atoms, respectively. e, f regions represented the N–H···π interaction and j can be speculated as dispersion interaction due to no electrostatic attraction between adjacent N–H and benzene ring showing in ESP-mapped molecular vdW surface images. Specific calculation methodology was described in Supplementary material. Here, in the cathodic ECL system, imprinted contours worked as capture sites and formed weak interactions with DA, thus further forming the OFF-type MIECLS by ECL quenching effect. The combination of the imprinted effect of MIP and quenching effect of o-benzoquinone species endowed the MIECLS with double recognition functions of DA sensing.

Multiple parameters in the process of MIECLS construction were evaluated to achieve the optimal ECL response. The proportion of PATP@AuNPs and DA affects the imprinted effect of the MIECLS. The amount of PATP@AuNPs within a certain range can assist the electronic transfer. While the overmuch stacking of PATP@AuNPs may interfere with ECL signal of UCNPs. As shown in Fig. S3, the maximum quenching value of ECL intensity occurred when the ratio of PATP@AuNPs and DA is 3:1, implying the optimum ECL effect was obtained at this proportion. Different time of extraction and rebinding process for MIECLS are also of significance to obtain the best analytical performance of MIECLS. Fig. S4 (green) shows clearly that the ECL values after elution was increasing before 15 min and then reached a plateau after 15 min. And the ECL intensities showed the upward trend with the rebinding time between 0 and 8 min, after which the intensities levelled out (purple). Here, 15 min and 8 min were selected as optimal elution time and rebinding time, respectively. Additionally, the pH of detection solution (0.1 M $K_2S_2O_8$) exerts a crucial effect on ECL performance. Fig. S5 shows that the ECL quenching values went up gradually from 5.4 to 7.4, and then showed a descending trend from 7.4 to 8.4, which demonstrated that the neutral pH was suitable for the rebinding process.

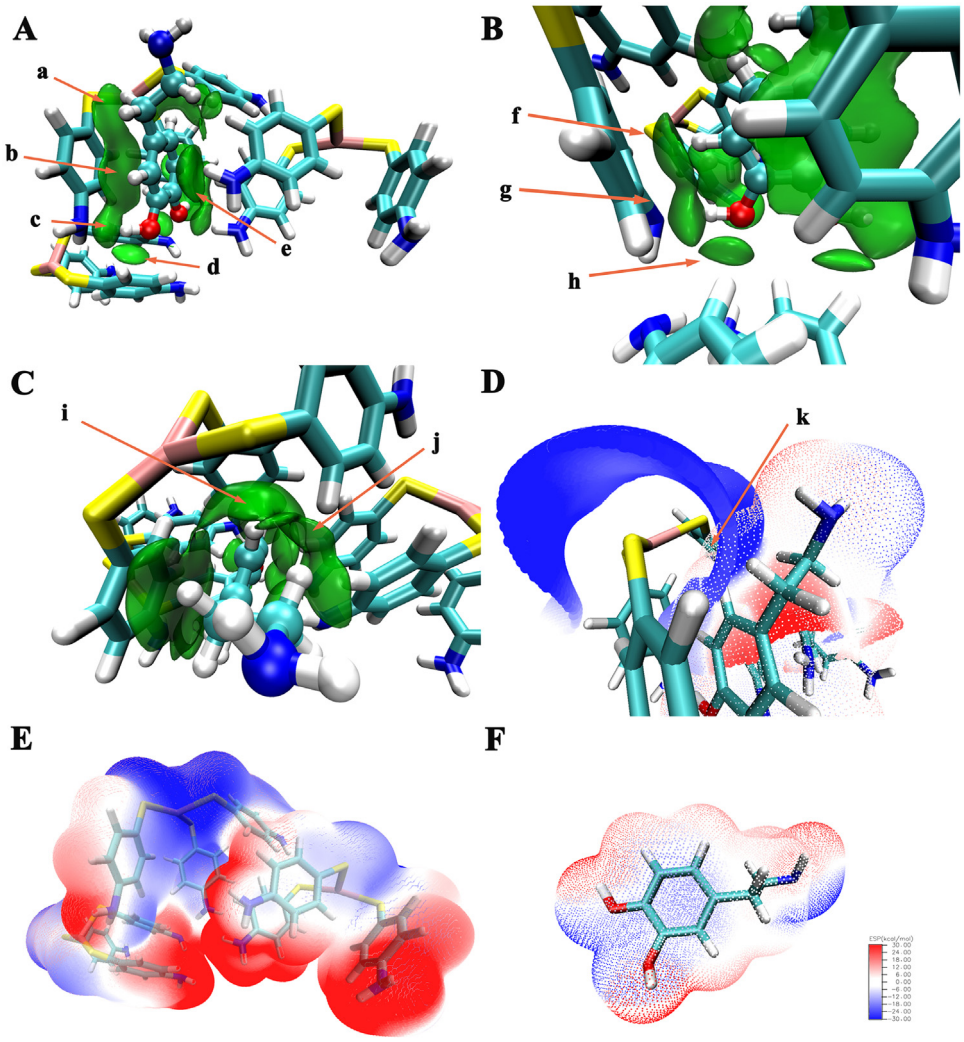

Fig. 2. (A), (B) and (C): the Independent Gradient Model (IGM) images of template and monomers at different views; ESP-mapped molecular vdW surface images of (E) functional monomers and (F) target, respectively and (D) partial image of target and monomers after shielding other areas (the unit: kcal/mol); different colors representing different atoms: Au (pink), S (gold), C (green), N (blue) and O (white). (For interpretation of the references to color in this figure legend, the reader is referred to the web version of this article.)

3.4. Light-emitting mechanism of the ECL system and quenching effect of DA towards MIECLS

Fig. 3A shows the photoluminescence (PL) and ECL spectra of $NaYF_4$:Yb,Tm UCNPs. Compared with PL spectrum (emitting at 475 nm), ECL spectrum of UCNPs centered on 490 nm presenting a little red shift, which was attributed to the different light-emitting mechanisms of ECL (Yin et al., 2012). For PL process, the emission peaks located at 475 nm corresponding to the $^1G_4 \rightarrow {}^3H_6$ transitions of Tm^{3+} (Jin et al., 2017; Lu et al., 2016). For ECL process, the $NaYF_4$:Yb,Tm was first reduced to negatively charged radical ($NaYF_4$:Yb,$Tm^{-\bullet}$) by the injection of energetic electron, in the wake of which the coreactant $S_2O_8^{2-}$ was reduced to the strong oxidant-anion sulfate radical ($SO_4^{-\bullet}$) (Gao et al., 2017). Subsequently, the $SO_4^{-\bullet}$ could further react with $NaYF_4$:Yb,$Tm^{-\bullet}$ to produce the excited form ($NaYF_4$:Yb,Tm*) followed by returning to ground state of $NaYF_4$:Yb,Tm* and releasing photons. The ECL process (Scheme 1C) was deduced as follows (Jin et al., 2018):

$$NaYF_4{:}Yb,Tm + e^- \rightarrow NaYF_4{:}Yb,Tm^{-\bullet} \quad (1)$$

$$S_2O_8^{2-} + e^- \rightarrow SO_4^{2-} + SO_4^{-\bullet} \quad (2)$$

$$NaYF_4{:}Yb,Tm^{-\bullet} + SO_4^{-\bullet} \rightarrow NaYF_4{:}Yb,Tm^* + SO_4^{2-} \quad (3)$$

$$NaYF_4{:}Yb,Tm^* \rightarrow NaYF_4{:}Yb,Tm + h\nu \quad (4)$$

In proposed strategy, we constructed a signal-off MIECLS for the DA detection. The quenching mechanism of DA towards MIECLS was also speculated (shown in Scheme 1D). It has been reported that DA itself is not the quencher of luminophore but the oxidative product of DA (*o*-benzoquinone species) (M. Zhao et al., 2016). The *o*-benzoquinone species could efficiently quench the ECL emission by energy transfer which derives from the collision between the excited state of UCNPs and the produced o-benzoquinone (Liu et al., 2007).

As shown in Fig. 3B, the CV curves of UCNPs modified electrode in 0.1 M PBS containing DA (b) did not show obvious redox peak, indicating the targets were not oxidized by electrochemical process. And after the adding of $K_2S_2O_8$ (c), CV profile showed a prominent peak at 1.75 V, demonstrating the oxidation of DA caused by $K_2S_2O_8$. The result was also validated by UV–vis spectra. Fig. 3C shows the UV absorption peak of DA in 280 nm. However, with the mixing of $K_2S_2O_8$ and DA solution, the peak at 280 nm was replaced by a new absorption peak appearing in 300 nm gradually indicating the generation of *o*-benzoquinone species. Hence, the oxidation of DA to yield the quencher of ECL was carried out by the adding of $K_2S_2O_8$. In this ECL system, the quenching mechanism can be speculated that targets were specifically adsorbed by PATP@AuNPs-crosslinked MIP contours at first and then

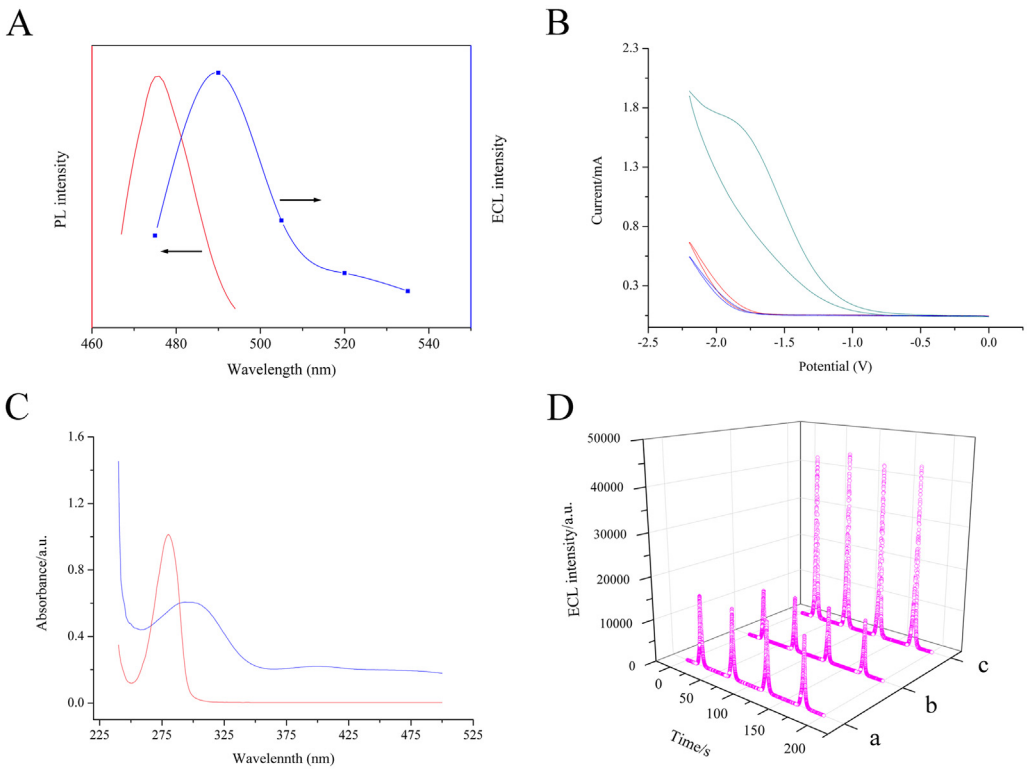

Fig. 3. (A) The PL spectrum (red) of UCNPs obtained with excitation wavelength 980 nm and the ECL spectrum (blue) of UCNPs modified electrode (B) CV curves of UCNPs modified electrode in 0.1 M PBS without (a) and with DA (b), and UCNPs modified electrode in 0.1 M $K_2S_2O_8$ with DA (c); (C) UV–vis spectra of DA in 0.1 M PBS (a) and 0.1 M $K_2S_2O_8$ in PBS solution (b); (D) ECL responses of NIP/UCNPs/CTpBD-Au/GCE (a), MIP/UCNPs/CTpBD-Au/GCE before (b) and after (c) the extraction. (For interpretation of the references to color in this figure legend, the reader is referred to the web version of this article.)

oxidized by $K_2S_2O_8$ to form *o*-benzoquinone species, thus causing the ECL quenching by energy-transfer process.

3.5. Analytical performance of the MIECLS

The ECL intensity of nonimprinted modified electrode (NIP/UCNPs/CTpBD-Au/GCE) and DA-imprinted modified electrode (MIP/UCNPs/CTpBD-Au/GCE) before and after the extraction process of DA were investigated to evaluate the imprinting performance of MIECLS. For MIP/UCNPs/CTpBD-Au/GCE (Fig. 3D), ECL intensity significantly recovered from ~12503 a.u. to ~45817 a.u. after extraction, suggesting the valid removal of the template (DA) from PATP@AuNPs-crosslinked MIP matrix. And compared with MIP-based electrode (before extraction), NIP/UCNPs/CTpBD-Au/GCE (a) obtained the higher intensity (~16472 a.u.). As reported in previous study (Yildiz et al., 2008), oligoaniline bridging units could serve as carrier of the electronic transfer in the ECL system by controlling their redox-state. Under the negative potential, oligoaniline bridge would be at their reduced state, in this case, instead of acting as electron acceptor they tunnel the electrons from the electrode through the AuNPs. Hence, the more PATP@AuNPs in NIP film could assist electron transport, thus obtaining higher ECL value. And the ECL curves of MIP/UCNPs/CTpBD-Au/GCE and NIP/UCNPs/CTpBD-Au/GCE for the detection of the same concentration of DA were shown in Fig. S6A and B, respectively. The quenching value of ECL obtained by MIP/UCNPs/CTpBD-Au/GCE was ca. ~21000 a.u. which was 20-fold than that of NIP/UCNPs/CTpBD-Au/GCE. The better quenching effect of MIP-based sensor was attributed to the specific affinity of recognition sites in PATP@AuNPs-crosslinked MIP matrix. The weak interactions of DA to the PATP@AuNPs-crosslinked MIP were synergistically stabilized by imprinted molecular contours to realize specific recognition. With the increase of DA, electrons were trapped more effectively resulting in an obvious quenching of ECL signals as expected.

As shown in Fig. 4B, MIECLS showed higher sensitivity than NIECLS, exhibiting good specificity towards DA. In other words, the favorable recognition capacity of PATP@AuNPs-crosslinked MIP and the quenching effect of *o*-benzoquinone species jointly realized quantitative determination of DA.

Fig. 4A shows the ECL intensity of a series of concentration of DA detected by MIECLS. The linear regression equation (Fig. 4B) of quantitative detection by MIECLS for DA (1×10^{-14}-1×10^{-6} M) was F_0-$F/F_0 = 0.06516 \lg C_{DA} + 0.98982$ with the correlation coefficient (R^2) of 0.9982 and the LOD of 2×10^{-15} M (S/N = 3).

3.6. Selectivity, stability and reproducibility

Selectivity reflects the recognition capacity of MIECLS towards DA. To assess the selectivity of the MIECLS, ECL responses were recorded by assaying the structurally analogues (Fig. S7) of DA (adrenaline, PEA and caffeic acid) and co-existing interferents (UA and AA) in rat serum. As shown in Fig. 4C, the ECL shift of MIECLS towards DA (10^{-9} M) is several-fold higher than other compounds. The *t*-test also confirmed the visible difference of sensing responses at MIP/UCNPs/CTpBD-Au/GCE towards interferents and DA (below the level of 0.01). The high selectivity of MIP was attributed to the complementary recognition sites in the PATP@AuNPs-crosslinked MIP contours matching the unique molecular structure of DA via multi-weak interactions. To evaluate the anti-interfering ability in ionic environment, Ca^{2+}, NH^{4+}, K^+, Na^+, SO_4^{2-}, NO_3^-, Cl^- were also tested with ten times concentration higher than DA. The ECL response of MIECLS towards DA (10^{-9} M) was similar to that toward the mixture of DA and ions (with the ratio of 96.70%), which implies the favorable anti-interfering ability of proposed MIECLS in ionic environment. To investigate the short-time stability (Fig. 4D) for developed MIECLS, consecutive detections (target concentration:10^{-10} M) for nine times were carried out. It was quite stable (with the SD below 3.0%) for several consecutive detections. The MIECLS also displayed favorable long-time stability (Fig. S8) after storage at 4 °C for 12 days. And the parallel detection result revealed high reproducibility (with the SD below 4.0%) for the five MIECLS (with the fixed DA concentration 10^{-10} M).

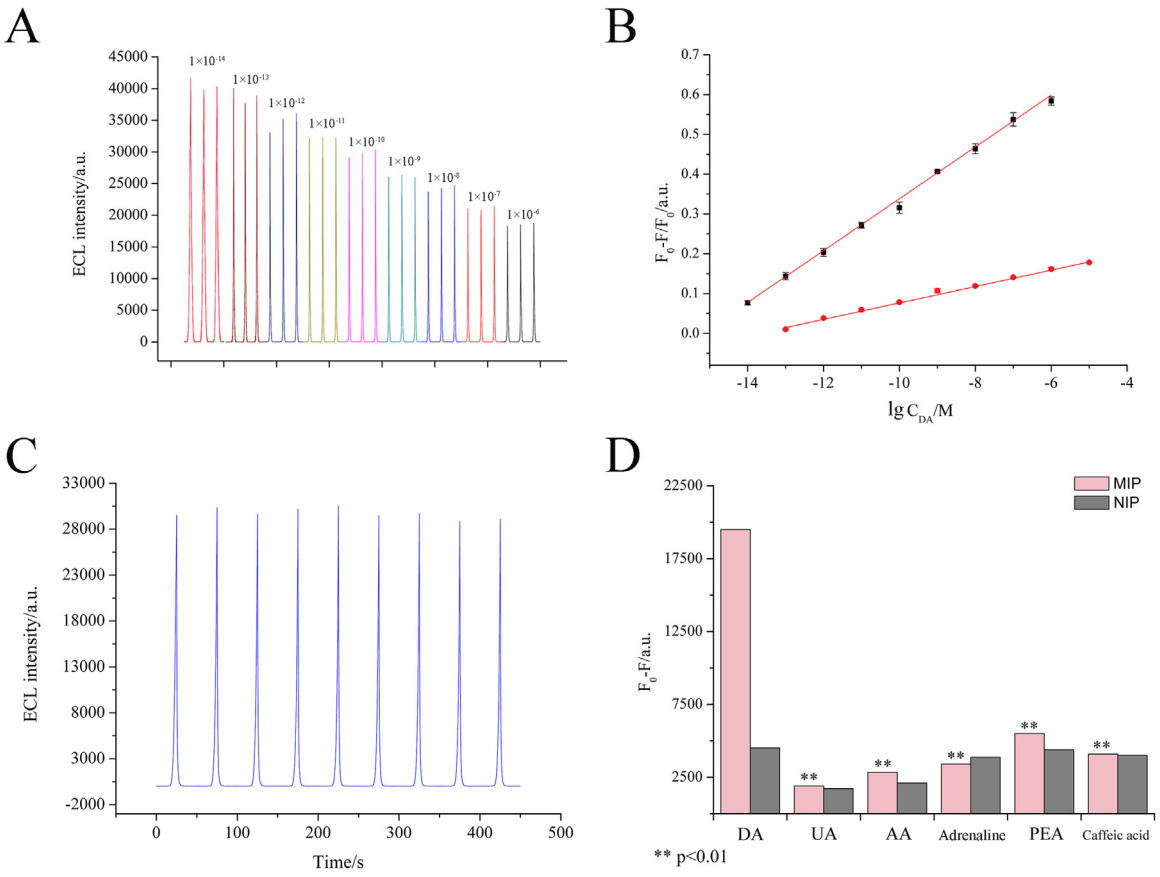

Fig. 4. (A) ECL curves of a series concentration of DA (1×10^{-14}–1×10^{-6} M) detected by MIECLS; (B) the calibration curve of proposed MIECLS and NIECLS for DA detection; (C) the specificity of the MIECLS towards DA and its interferents with the same concentration; (D) the ECL profile for several consecutive detections carried out by MIECLS.

3.7. Application of the ECL sensor in samples

It has been reported that the concentration of DA in human serum should be below 0.9×10^{-9} M (Fu et al., 2017) and the abnormal DA level may cause various pathosis. In this study, trace amounts of DA were added into rat blood samples for the spiked sample recovery test. The bloods were then repeatedly centrifuged at 2000 rpm for 20 min to collect serum. Subsequently, methanol was added into serum at ratio of 1:1 (v/v) in order to remove proteins (Li et al., 2016). The final supernatant was used for MIECLS detection. As shown in Table 1, the obtained recoveries of spiked DA standard solutions in serum samples at three different concentration levels were 93.25–112.97% (with RSDs below 3.0%), suggesting the feasibility of the MIECLS for the determination of DA in serum sample.

4. Conclusion

In this work, the novel COF-based material (CTpBD-Au) to enhance ECL of UCNPs and PATP@AuNPs-crosslinked imprinting recognition sites to specifically bind the targets were introduced to MIECLS for the determination of DA in rat serum samples. The COFs-based ECL enhancement material could hold more UCNPs for ECL and PATP@AuNPs-crosslinked MIP contours with DA recognition sites. AuNPs loaded on COFs enabled the hybrid to tunnel the electrons between electrodes and UCNPs. And with the assistance of three-dimensional molecularly imprinted contours and the conductivity of PATP@AuNPs-crosslinked MIP matrix, the ECL sensing effect was further enhanced. The molecularly imprinted contours could interact with DA through multiple weak interactions. A double recognition effect was realized by the recognition effect of MIP and the quenching effect of *o*-benzoquinone species for MIECLS. The proposed MIECLS showed a wide detection range, low limit of detection and acceptable recoveries in rat serum sample, suggesting its promising application in practical detection.

Table 1
Recoveries of DA in spiked samples detected by proposed method.

Samples	Spiked concentration (mol L^{-1})	Detection concentration (mol L^{-1} n = 3)	RSD (%)	Recovery (%)
Serum 1	10^{-11}	0.9337×10^{-11}	2.15	93.34
	10^{-10}	0.9736×10^{-10}	2.14	97.36
	10^{-9}	1.1297×10^{-9}	2.23	112.97
Serum 2	10^{-11}	0.9325×10^{-11}	2.56	93.25
	10^{-10}	0.9616×10^{-10}	1.15	96.16
	10^{-9}	1.0781×10^{-9}	2.80	107.81

Acknowledgements

This work was supported by "The National Key R&D Program of China" (No. 2016YFD0401202); and the Special Project of Tianjin Innovation Platform (No. 17PTGCCX00230).

Appendix A. Supporting information

Supplementary data associated with this article can be found in the online version at https://doi.org/10.1016/j.bios.2018.12.043.

References

Anirudhan, T.S., Alexander, S., Lilly, A., 2014. Polymer 55, 4820–4831.
Ding, S.Y., Gao, J., Wang, Q., Zhang, Y., Song, W.G., Su, C.Y., Wang, W., 2011. J. Am. Chem. Soc. 133, 19816–19822.
Fu, X., Tan, X., Yuan, R., Chen, S., 2017. Biosens. Bioelectron. 90, 61–68.
Gao, N., Ling, B., Gao, Z., Wang, L., Chen, H., 2017. Anal. Bioanal. Chem. 409, 2675–2683.
Guo, X., Wu, S., Duan, N., Wang, Z., 2016. Mn(2+)-doped Anal. Bioanal. Chem. 408, 3823–3831.
Huang, Z., Wu, S., Duan, N., Hua, D., Hu, Y., Wang, Z., 2012. J. Pharm. Biomed. 66, 225–231.
Humphrey, W., Dalke, A., Schulten, K., 1996. J. Mol. Graph. 14, 33–38.
Jiang, M., Braiek, M., Florea, A., Chrouda, A., Farre, C., Bonhomme, A., Bessueille, F., Vocanson, F., Zhang, A., Jaffrezic-Renault, N., 2015. Toxins 7, 3540–3553.
Jin, L.M., Chen, X., Siu, C.K., Wang, F., Yu, S.F., 2017. ACS Nano 11, 843–849.
Jin, X., Fang, G., Pan, M., Yang, Y., Bai, X., Wang, S., 2018. Biosens. Bioelectron. 102, 357–364.
Jo, E.J., Mun, H., Kim, M.G., 2016. Anal. Chem. 88, 2742–2746.
Lefebvre, C., Rubez, G., Khartabil, H., Boisson, J.C., Contreras-García, J., Hénon, E., 2017. Phys. Chem. Chem. Phys. 19, 17928–17936.
Li, Y., Song, H., Zhang, L., Zuo, P., Ye, B.-C., Yao, J., Chen, W., 2016. Biosens. Bioelectron. 78, 308–314.
Liu, T.Z., Hu, R., Zhang, X., Zhang, K.L., Liu, Y., Zhang, X.B., Bai, R.Y., Li, D., Yang, Y.H., 2016. Anal. Chem. 88, 12516.
Liu, X., Jiang, H., Jianping Lei, A., Ju, H., 2007. Anal. Chem. 79, 8055–8060.
Lu, T., Chen, F., 2012. J. Comput. Chem. 33, 580–592.
Lu, Z., Wang, J., Li, R., Qiao, Y., Zhou, M., Li, C.M., 2016. Nanoscale 8, 18524–18530.
Neese, F., 2012. J. Chem. Phys. 2, 73–78.
Pachfule, P., Kandambeth, S., Díaz Díaz, D., Banerjee, R., 2014. Chem. Commun. 50, 3169–3172.
Qian, H.L., Yang, C.X., Yan, X.P., 2016. Nat. Commun. 7, 12104.
Riskin, M., Telvered, R., Bourenko, T., Granot, E., Willner, I., 2008. J. Am. Chem. Soc. 130, 9726–9733.
Sheikhzadeh, E., Chamsaz, M., Turner, A.P., Jager, E.W., Beni, V., 2016. Bioelectronics 80, 194–200.
Wang, Z., Qian, Y., Wei, X., Zhang, Y., Wu, G., Lu, X., 2017. Electrochim. Acta 250, 309–319.
Wu, Z., Li, H., Liu, Z., 2015. Sens. Actuators B-Chem. 206, 531–537.
Xue, C., Han, Q., Wang, Y., Wu, J., Wen, T., Wang, R., Hong, J., Zhou, X., Jiang, H., 2013. Biosens. Bioelectron. 49, 199–203.
Yang, J.J., Cao, J.T., Wang, H., Liu, Y.M., Ren, S.W., 2017. Talanta 167, 325–332.
Yang, Y., Fang, G., Wang, X., Liu, G., Wang, S., 2016. Biosens. Bioelectron. 77, 1134–1143.
Yildiz, H.B., Tel-Vered, R., Willner, I., 2008. Adv. Funct. Mater. 18, 3497–3505.
Yin, M., Wu, L., Li, Z., Ren, J., Qu, X., 2012. Nanoscale 4, 400–404.
Zhang, J., Wang, C., Niu, Y., Li, S., Luo, R., 2017. Sens. Actuators B-Chem. 249, 747–755.
Zhao, L., Li, J., Liu, Y., Wei, Y., Zhang, J., Zhang, J., Xia, Q., Zhang, Q., Zhao, W., Chen, X., 2016a. Sens. Actuators B-Chem. 232, 484–491.
Zhao, M., Chen, A.Y., Huang, D., Zhuo, Y., Chai, Y.Q., Yuan, R., 2016b. Anal. Chem. 88, 11527–11532.
Zhong, M., Teng, Y., Pang, S., Yan, L., Kan, X., 2015. Biosens. Bioelectron. 64, 212–218.